Title:	Post-tensioned girders with low amounts of shear reinforcement: Shear strength and influence of flanges
Authors:	Rupf M., Fernández Ruiz M., Muttoni A.
Published in:	Engineering structures
DOI	10.1016/j.engstruct.2013.05.024
Pages:	15 p.
Year of publication:	2013
Type of publication:	Peer reviewed journal article

Please quote as:	Rupf M., Fernández Ruiz M., Muttoni A., *Post-tensioned girders with low amounts of shear reinforcement: Shear strength and influence of flanges*, Engineering structures, 2013, 15 p..

Engineering Structures 56 (2013) 357–371

Contents lists available at SciVerse ScienceDirect

Engineering Structures

journal homepage: www.elsevier.com/locate/engstruct

Post-tensioned girders with low amounts of shear reinforcement: Shear strength and influence of flanges

Michael Rupf, Miguel Fernández Ruiz *, Aurelio Muttoni

Ecole Polytechnique Fédérale de Lausanne, Station 18, CH-1015 Lausanne, Switzerland

ARTICLE INFO

Article history:
Received 21 February 2013
Revised 8 May 2013
Accepted 13 May 2013

Keywords:
Shear design
Prestressed concrete
Post-tensioning
Experimental programme
Stress fields
Girder flanges

ABSTRACT

Assessing the strength of existing structures has become a major issue for structural engineers. Such analyses are often performed after changes of use of the structure or due to new design codes requirements. This is particularly relevant with respect to the shear strength of post-tensioned concrete bridges. Such structures were often designed in the past with fairly low amounts of shear reinforcement and do not comply with current code requirements in terms of amount of transverse reinforcement or shear strength. However, it should be noted that codes of practice cover the design of a wide range of cases and sometimes neglect some load-carrying actions or may be too conservative for assessing others. Therefore, the use of more refined models may potentially increase the predicted shear resistance and avoid unnecessary strengthening of existing structures. In this paper, an investigation on the behaviour of post-tensioned beams with low amounts of shear reinforcement and flanges is presented. First, the results of an experimental programme on twelve reinforced concrete beams (10.0 m long, 0.78 m high) failing in shear are described. The test series is used to analyse the most significant parameters influencing the shear strength and the failure modes. Its results are compared to a number of design codes showing different levels of accuracy. The test results are finally compared to the results of analyses based on elastic–plastic stress fields. This technique shows excellent results when compared to the test results and allows investigating on the role of the various shear-carrying actions, of the prestressing level and on the transverse reinforcement amount with respect to the various potential failure modes.

1. Introduction

Prestressing enables simple and economic construction of medium to large span concrete structures providing sufficient strength at ultimate and controlling the deflections and cracking state under serviceability conditions. Therefore, a large number of thin-webbed concrete girders have been built in the second part of the last century by using this technique. Design of these members has significantly evolved, from analyses of the stress state under service loads to equilibrium-based models at ultimate limit state. The evolution of design models as well as changes in actions and/or geometry (deck slab widening or others) require often the assessment of the performance of such existing bridges. This task frequently shows insufficient shear strength for existing members assessed with modern codes due to too low amounts of available shear reinforcement or insufficient stirrup anchorage and leads in many cases to expensive retrofitting of existing bridge girders. However, it should be noted that design codes are usually intended for design of a wide number of structures with a sufficient level of safety. For instance, for prestressed bridges, a number of shear carrying actions are usually neglected or estimated in a coarse (excessively safe) manner. This is the case of the shear force carried by flanges, the effective concrete strength at web crushing, the increase of the stress in the tendons, or the minimum allowable angle of the compression field in the web.

The behaviour of prestressed girders with varying amounts of shear reinforcement has previously been investigated by a number of researchers [1–10], mostly by testing simply supported members. However, the behaviour of prestressed continuous beams and the influence on their behaviour of flanges as well as detailing of the stirrups has been poorly addressed in the past. Nevertheless, these members are representative of continuous box-girder bridges, widely used in current practice particularly for long spans. In order to investigate more in detail the behaviour and strength of these members, a test series on twelve reinforced concrete beams was carried out at the Ecole Polytechnique Fédérale de Lausanne, Switzerland. The main parameters of the test series are the shear reinforcement ratio, the amount of post-tensioning force, the cross section shape and the stirrup anchorage detailing. The present paper describes the test series and its main results. The prediction of the behaviour of the test specimens has been done for a number of design codes as well as by using the elastic–plastic stress field

* Corresponding author. Tel.: +41 21 693 28 89; fax: +41 21 693 58 84.
E-mail addresses: michael.rupf@epfl.ch (M. Rupf), miguel.fernandezruiz@epfl.ch (M. Fernández Ruiz), aurelio.muttoni@epfl.ch (A. Muttoni).

0141-0296/$ - see front matter © 2013 Elsevier Ltd. All rights reserved.
http://dx.doi.org/10.1016/j.engstruct.2013.05.024

Nomenclature

A	cross section area of the beam in the testing region
E_c	Young's modulus for the concrete
E_s	Young's modulus for the rebar steel or the prestressing strand
P	nominal post-tensioning force
P_{test}	post-tensioning force at the testing day
Q	applied load at the cantilever
R	radius for the deviation of the prestressing tendon
V	shear force
V_P	shear force carried by the prestressing tendon
V_R	shear strength
$V_{R,test}$	resulting shear strength of the tests
$V_{R,model}$	resulting shear strength of a model analysis
$V_{res,test}$	residual shear strength (calculated at twice the deflection at peak shear strength)
V_{bot}	shear force carried by the bottom flange
V_{top}	shear force carried by the top flange
V_w	shear force carried by the web
d	effective depth to main tension reinforcement
d_g	maximum aggregate size of the concrete
f_c	concrete compressive strength (cylinder)
f_{cm}	average concrete compressive strength at the testing day (cylinder)
f_{ctm}	average concrete tensile strength at the testing day (direct tensile test)
f_y	yield strength of the rebar steel or the prestressing strand
f_t	ultimate tensile strength of the rebar steel or the prestressing strand
s	spacing of the rebars
t	crack opening
t_w	web thickness
$t_{w,eff}$	effective web thickness with reduction due to the prestressing tendon
v	deflection at the loading point in the span
w	opening of the crack normal to the crack surface
z	lever arm of the internal forces
Δ	sliding of the crack parallel to the crack surface
ΔV_P	increase in shear force carried by the prestressing tendon
Δt_w	increase in web thickness
$\Delta\varphi$	unintended deviations per unit length for the prestressing tendon
$\Delta\varepsilon_P$	increase in strain of the prestressing tendon
β_P	inclination of the prestressing tendon
ε_u	ultimate strain of the rebar steel or the prestressing strand
ε_x	strain in the horizontal direction (x)
ε_z	strain in the vertical direction (z)
ε_2	concrete compressive strain in the principal direction
η_{fc}	strength reduction factor to account for the brittleness of high strength concrete
η_ε	strength reduction factor to account for the tensile strains in transverse direction to the compression
θ_{crack}	measured angle of cracks in the testing region
θ_σ	inclination of the principal concrete compressive stress
θ_ε	inclination of the principal concrete compressive strain
μ	frictional coefficient for prestressing tendons in the steel duct
ρ_w	shear reinforcement ratio in the testing region
σ_c	concrete compressive stress in the principal direction
τ_{xy}	concrete shear stress in the direction of the girder axes
υ	direction of the crack opening with respect to the normal direction of the crack surface
Ø	diameter of the reinforcement bar or the prestressing strand
Avg	average
CoV	coefficient of variation
LoA	level of approximation

method (EPSF). This latter method was developed by Fernández Ruiz and Muttoni [11] and can be considered as an enhancement of the rigid-plastic stress fields (refer for instance to Muttoni et al. [12]). The EPSF method is solved by using the finite element method and allows accounting for compatibility conditions in a reinforced concrete element as well as for the role of transverse cracking on the concrete strength [13]. A comparison of the test results with the model prediction of the EPSF method is presented in this paper, showing an excellent agreement and allowing to investigate the role of the various shear carrying actions and failure modes.

2. Experimental programme

A test series on twelve reinforcement concrete beams was performed to investigate the behaviour of continuous bridge girders with low amounts of shear reinforcement (ρ_w defined as the ratio between the cross section of the transverse reinforcement and the corresponding web area), different ratios of post-tensioning (defined as the ratio between the post-tensioning force P and the concrete gross cross section A), and different cross sections (with and without flanges). The three main parameters refer to the testing region and their nominal values are listed in Table 1. The static system of the test setup corresponds to a single span beam with a cantilever and represents the situation of a continuous bridge girder near an inner support (refer to Fig. 1). The test specimens correspond thus to the girders of a multi-span bridge with a span length of about 40 m at a scale 3/8.

2.1. Specimens

All test specimens are 10 m long and 780 mm high and present in the central part a testing region with a length of about 4.80 m (refer to Fig. 2). Ten beams are casted as girders with two flanges (cross section according to the tests in [7]) and the remaining two without flanges (rectangular cross section). All flanged beams have a web thickness of 150 mm in the testing region and 400 mm in the external parts (to avoid shear failure), and a flange width of 800 mm. The web thickness of the two rectangular beams is also 150 mm in the testing zone and 300 mm outside.

The shear reinforcement ratio ρ_w varies between 0.063% and 0.251% for the different specimens and refer to the testing region in the centre of the beam. It can be noted that for $\rho_w = 0.063\%$ the reinforcement amount is lower than the minimum one prescribed usually in codes (in Model Code 2010 [14] for instance, $\rho_{w,\min} = 0.08 \cdot \sqrt{f_c}/f_y \approx 0.08\%$ for the investigated tests). Fig. 2b and c shows the reinforcement layout where the shear reinforcement in the central part is composed of stirrups with different anchorage conditions or links which are installed in alternating locations (opposite sides of the web). The longitudinal reinforcement consists of straight bars over the whole length of the girder. The design of the stirrups and links, their diameter and spacing,

Table 1
Main parameters (ρ_w and P/A refer to nominal values in the testing region), reinforcement layout (Fig. 2, dimensions in mm, note: links in alternating position), measured concrete properties (f_{cm} and f_{ctm} at the day of the test, E_c at 28 days after casting of the specimen), dates (days after casting of the specimen) and effective ratio of prestressing.

		Nominal values					Actual values					
Beam	Cross section	ρ_w [%]	P/A [MPa]	Transverse reinforcement	Longitudinal reinforcement Layer 1	Layer 2	f_{cm} [MPa]	f_{ctm} [MPa]	E_c [MPa]	$t_{prestressing}$ [days]	t_{test} [days]	P_{test}/A [MPa]
SR21	I	0.086	2.5	Ø6 @220	4Ø26 + 6Ø18	8Ø10	30.8	2.6	29’700	22	36	2.40
SR22	I	0.126	2.5	Ø6 @300	4Ø26 + 6Ø18	8Ø10	33.7	3.1	31’950	35	79	2.38
SR23	I	0.063	2.5	Ø6 @300	4Ø26 + 6Ø18	8Ø10	35.3	3.7	30’250	42	58	2.45
SR24	I	0.251	2.5	Ø6 @150	4Ø26 + 6Ø18	8Ø10	31.3	2.8	28’050	28	59	2.38
SR25	I	0.086	5.0	Ø6 @220	4Ø26 + 6Ø10	8Ø10	33.1	3.1	32’700	19	47	4.73
SR26	I	0.063	5.0	Ø6 @300	4Ø26 + 6Ø10	8Ø10	36.9	3.5	31’600	39	68	4.82
SR27	I	0.188	5.0	Ø6 @200	4Ø26 + 6Ø10	8Ø10	28.3	2.9	27’450	35	53	4.85
SR28	I	0.086	-	Ø6 @220	4Ø26 + 6Ø10	8Ø10	37.8	4.0	31’250	-	90	-
SR29	I	0.251	2.5	Ø6 @150	4Ø26 + 6Ø18	8Ø10	29.8	2.8	27’800	26	65	2.36
SR30	I	0.251	2.5	Ø6 @150	2Ø26 + 4Ø10	6Ø10	31.4	3.5	30’300	15	79	2.28
SR31	I	0.086	3.0	Ø6 @220	2Ø26	2Ø10	31.3	2.7	31’550	16	31/35	2.93
SR32	I	0.086	-	Ø6 @220	2Ø26	2Ø26	35.2	3.4	33’400	-	42	-

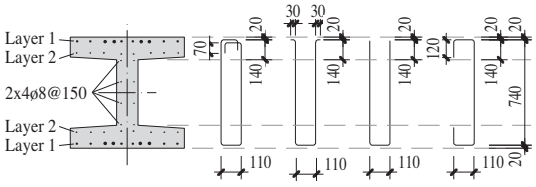

and the amount of longitudinal reinforcement in the flanges are detailed in Table 1. The Table also shows the detail for stirrup anchorage of the three beams SR24, SR29, and SR30.

Ten beams are post-tensioned with a nominal longitudinal stress P/A of 2.5, 3.0 or 5.0 MPa which refers to the testing zone. The girders with the higher prestressing (5.0 MPa) contain two tendons with four strands 150 mm^2 each and the other prestressed specimens one tendon of the same type (4 strands150 mm^2). All tendons are placed in ribbed steel ducts 45/50 mm (inner/outer diameter) which are grouted with a high strength mortar after prestressing. On both sides, active anchorage heads are placed, although only one was used for prestressing. The tendon layout follows the bending moments of the external loads and presents two circular curved deviations and straight segments elsewhere. The two types of post-tensioning layout for one or two tendons are presented in Fig. 3.

The tendons were stressed at 1395 MPa (75% of their tensile strength). The actual prestressing force in the testing region accounting for friction losses (assumed: $\mu = 0.18$; $\Delta\varphi = 0.005$ m^{-1}), wedge drawn-in and time-delayed losses (creep, shrinkage, relaxation) has been calculated according to Model Code 2010 [14]. The results were checked against measurements of concrete strains (glued strain gauges on the specimen) with good agreement. The resulting (calculated) average values of prestressing stress P_{test}/A acting in the testing region at the time of testing are provided in Table 1.

2.2. Test setup

The test setup is presented in Fig. 2 (a). The test specimens are supported on two mechanical bearings with a span of 7.20 m ($x = 200$ and $x = 7400$ mm) and are loaded at the cantilever ($x = 9800$ mm) and at one third of the inner span ($x = 2600$ mm). All supports and loading points allow the rotation around the z-axis. The bearing on the south direction is fixed in longitudinal direction whereas the support on the north direction and the two loading points allow longitudinal displacements. Loading is applied by means of hydraulic jacks, with the load applied in the span being twice the load at the cantilever. The shear force V in the testing region corresponds to the applied load at the cantilever Q (neglecting self-weight, refer to Fig. 1). The load configuration leads to a change of sign in the bending moments, with the point of contraflexure located in the middle of the testing region. The load is applied in several load steps with a loading rate for Q of 15 kN/min. before peak load (force controlled) and a rate of about 2.5 mm/min. afterwards (displacement controlled). At every load step, the deformation is kept constant for a couple of hours to perform the manual measurements.

2.3. Material properties

Normal strength concrete was used with a maximum aggregate size of 16 mm. Table 1 summarises the concrete compressive strength at the testing day f_{cm} (measured on cylinders 160 × 320 mm) and the tensile strength f_{ctm} (direct tensile test on cylinders 160 × 320 mm). Table 2 shows the material properties of the rebars and the strands used. All rebars between diameter 6 mm and 18 mm consist of normal strength reinforcement steel with low or normal ductility, whereas the rebars diameter 26 mm consist of a high strength reinforcement steel. The yield strength f_y of cold worked and high strength steel is defined at 0.2% residual strain whereas for the strands of the prestressing tendons it is defined at the 0.1% residual strain (according to Model Code 2010 [14]).

2.4. Measurements

The measurement system is the same for all specimens. A number of devices were used for continuous data acquisition comprising load cells, displacement transducers, inclinometers and glued gages allowing for the following measurements:

- Force at the two loading points and reaction at the supports measured by load cells.
- Vertical deflection measured by inductive displacement transducers between the bottom surface of the girder and the strong floor.
- Change of web thickness in the testing region measured by out-of-plane inductive displacement transducers.
- Elongation of the prestressing tendon measured by strain gauges glued to 8 mm studs (350 mm long, with end anchorage plates) arranged in the concrete outside the steel duct (3 measurements per specimen).

The load is applied in several load steps. After the load is increased at each load step, the following manual measurements are recorded:

- Deformation of the web and the flanges in the testing region measured by a demec device on a triangular truss system with an initial measurement length of 110 mm.
- Photos of the crack pattern on the girder.
- Measurement of the representative crack openings.

2.5. Test results

All specimens failed in shear in the testing region. Only the girder SR31 could be externally reinforced after failure on one side and tested a second time under the name SR31B. The ultimate shear strength $V_{R,test}$ (peak load) and the residual strength $V_{res,test}$ (measured at twice the deflection at peak load), are listed in Table 3. Three different failure modes can be observed in the test series. Fig. 4 shows the final crack pattern of three typical specimens failing in a different manner (failure modes for all specimens given in Table 3). The measured shear strength V and deflection under the loading point in the span v (at x = 2600 mm) for these specimens are also plotted in Fig. 4. The first type of failure is observed in girders with flanges and low amounts of shear reinforcement as SR21. It is characterised by an in-plane failure associated to large crack openings in several cracks of the web and by the development of delamination cracks at the interface of the flanges. At failure, rupture of the stirrups in tension developed. A rather constant residual strength develops for a load level between 59% and 80% of the ultimate strength (Table 3). The increase in web thickness (associated to a spalling failure of concrete) for these specimens (refer to Fig. 5 (a)) is quite limited before peak load is attained and even remains moderate with decreasing load. Increasing is only noticeable for very large displacements due to tendon's dowel action (refer to Fig. 4a). The second failure mode can be observed in flanged girders with higher amounts of shear reinforcement as SR24. It is associated to an out-of-plane failure of concrete with cover spalling out of the web along the tendons, followed by rupture of the stirrups. The residual strength remains also between 67% and 79% of the ultimate strength, with a slight tendency to soften as the member deflects. Fig. 5a shows clearly the spalling of the concrete cover by an increase of the web thickness when reaching the peak load. The third failure mode is associated to the beams without flanges as SR31. These girders show a brittle failure with the localisation of the strains in one single crack and residual strength between 30% and 39% of the ultimate strength. No significant increase in web thickness can be observed (Fig. 5a). Specimen SR26 failed in a combination of the first two failure modes with cover spalling at the tendons and development of delamination cracks (refer to Table 3).

As previously described, the test results show a significant influence of the amount of shear reinforcement and the post-tensioning ratio on the failure mode and on the ultimate strength. The presence of beam flanges turned out to be very beneficial, leading to larger shear strength and allowing the member to develop large deformations and significant residual strength. All flanged girders failed in the region of the point of contraflexure (Fig. 4a and b) whereas all girders without flanges failed due to a critical crack near load or support (Fig. 4c).

For all girders with prestressing tendons, an increase of the strain in the direction of the cable axis could be measured (Fig. 5b). This indicates therefore a beneficial increase of the prestressing force in the testing region. An influence of the stirrup anchorage conditions on the shear strength, the failure mode or the general behaviour of the girders was not observed. Nevertheless, this observation cannot be generalised to any anchorage detail, girder geometry and actions (specific investigations are still required for a general conclusion).

2.6. Results of strain measurements

The strains in the testing region are determined by means of the demec measurements on the web and on the two flanges. The demec readings begin with the application of the external load which means that the strains due to the prestressing and its losses are not accounted. Fig. 6 presents the measured strain profiles of the girders SR21, SR24 and SR31 which are representative of the three described failure modes. The profiles show the vertical strains ε_z at load levels between 52% and 100% of the peak load. It can be noted that in all cases the measurements are strongly influenced by the large opening of the actual cracks. A comparison of the vertical strain profiles of the three beams SR21, SR24 and SR31 show that cracks with significant openings develop over the whole testing region for the girder SR24 (Fig. 6b) whereas the vertical strains in the girders SR21 and SR31 (Fig. 6a and c) are more localised. At the last load step, the vertical strains exceed in most profiles 10‰ and can reach values of about 30‰ indicating large crack opening and extensive stirrup yielding (basis length of the demec measurement of 110 mm).

Fig. 6d–f shows for the girders SR21, SR24 and SR31 the measured principal compressive strain ε_2 at the last load step. The strains are only plotted where the measurements are unaffected by the presence of cracks developing through the measurement mesh. In the web of the girder SR21 a maximum compressive strain of 0.7‰ can be found in the middle of the beam at the level of the tendon. Larger strains were however recorded for specimen SR24 reaching 1.9‰ in the tendon region where crushing developed. For specimen SR31 (without flanges), the maximum compressive strains were also quite high (2.5‰). It should be noted for this specimen that the maximum strains are developed in the region of the compression chord and that the strains are quite low in other regions.

The inclination θ_ε of the principal compressive strain in the central part of the web (uncracked concrete struts, angle of blue lines in Fig. 6d–f with respect to the beam axis) can locally reach 10° with an average value of about 15° for specimen SR21 (values accounting for the results of the whole web; more details on these measurements are provided later). Other specimens failing in the same manner (large crack opening) show similar results. For the specimens where out-of-plane failure occurred along the tendon region (as specimen SR24), the inclination θ_ε of the compressive strains reach locally 14° and show an average value of about 22° (more details are provided later). For the two beams without

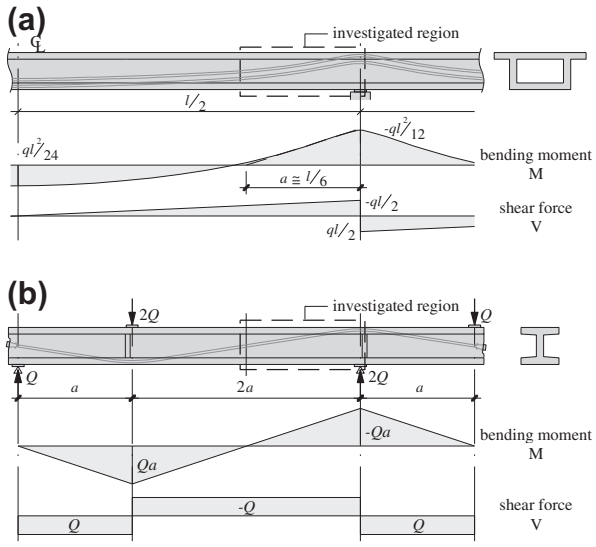

Fig. 1. Static system and internal forces of (a) a continuous box girder bridge under uniformly distributed loads and (b) test setup (self-weight neglected).

flanges, the inclination θ_ε of the compressive strains varies significantly over the length and the height of the girder.

It can be noted that the measured angles of the principal compressive strain θ_ε are significantly lower than the observed angle of the cracks θ_{crack} (Fig. 4). Cracking develops in the middle of the testing region at a fairly constant angle and appears for the first time for moderate to high load levels (50–85% of the maximum load). For all specimens the observed angle θ_{crack} varies between 19° and 26° in the testing region with somewhat flatter angles for members with higher level of post-tensioning. Nevertheless, the observed scatter does not allow deriving a clear correlation.

The measurements on the demec grid allow also investigating on the crack openings and their kinematics (by assuming the behaviour of the two parts separated by a crack behaving as rigid bodies). To do so, the actual crack shape is approximated by a polygonal line, whose keypoints are defined with a spacing equal to the aggregate size of the concrete (d_g = 16 mm, in case that the distance between the polygonal line and the actual crack is larger than half the aggregate size, an additional keypoint is introduced to correct it). The maximum crack opening thus obtained at the last load step before peak load is 2.0 mm for beam SR21 and 2.5 mm for beam SR24, which finely agrees with the direct measurements of the crack widths recorded during the tests. Performing this analysis of the demec measurements over all tested specimens leads to maximum crack openings of 4.5 mm for the beam SR28, followed by 3.5 mm for SR23 and between 2.0 and 2.5 mm for the other beams. The maximum crack opening of the two beams without flanges is 1.5 mm for the girder SR32 and 1.0 mm for the beam SR31 indicating that opening of the cracks in the web is relatively critical for these latter specimens.

Fig. 7a–c shows the kinematics for some selected cracks of the girders SR21, SR24 and SR31. The kinematics is drawn for the cracks in the region where the failure occurs and includes all load

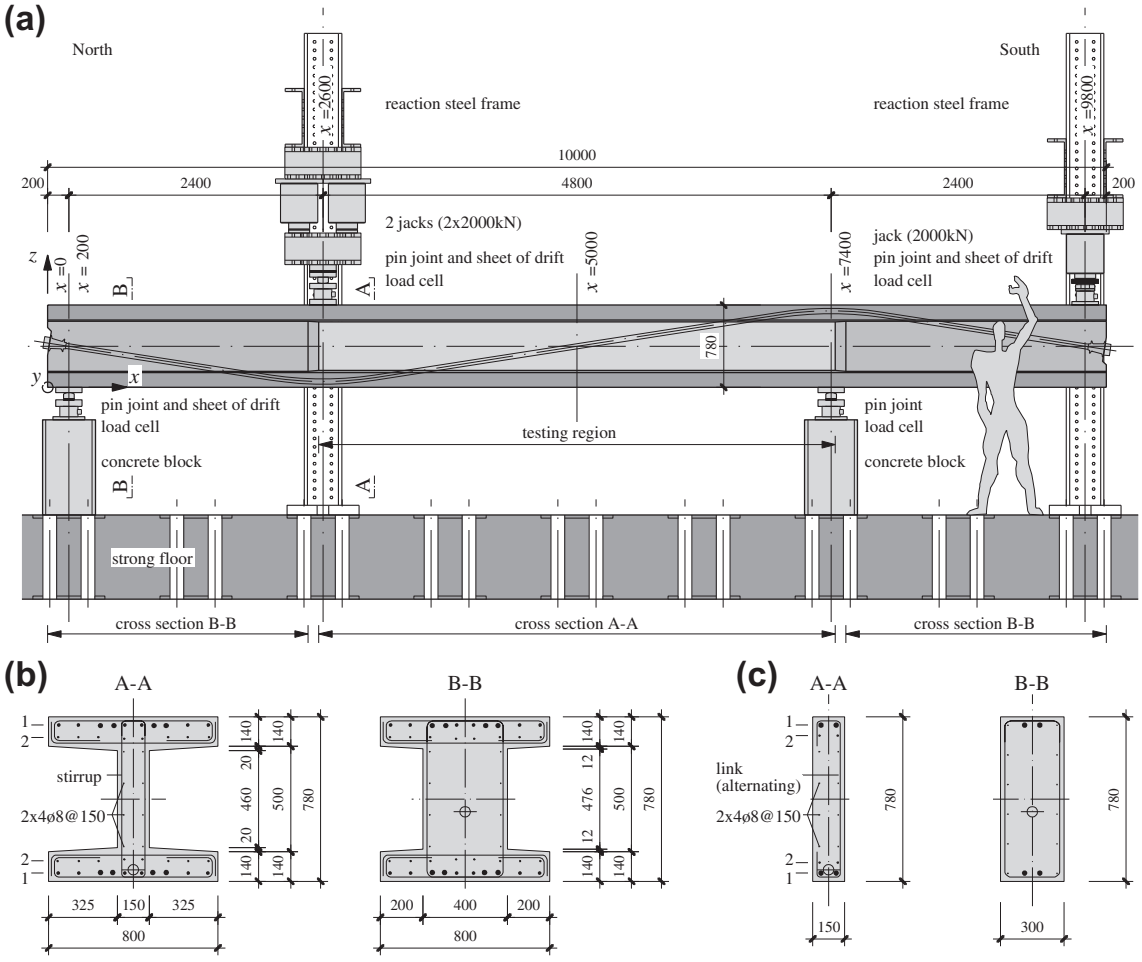

Fig. 2. Test setup, geometry and reinforcement of the specimens (dimensions in mm): (a) longitudinal view on the test setup; (b) cross sections of beams with flanges; (c) cross sections of beams without flanges. Reinforcement layers 1 and 2: see Table 1.

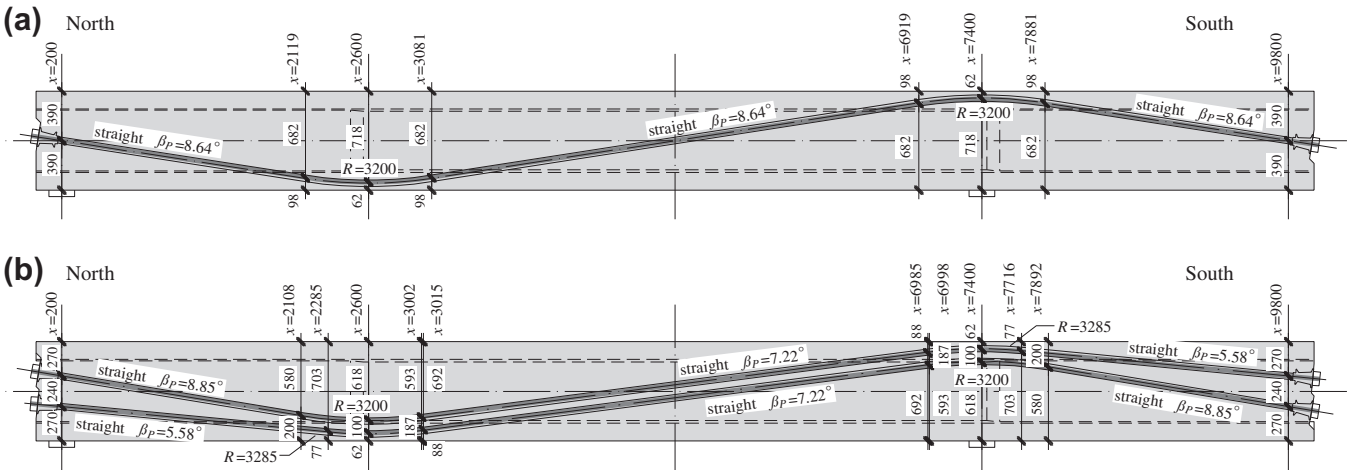

Fig. 3. Post-tensioning layout (dimensions in mm): tendon geometry (centre of gravity of the tendon) of girders with (a) one tendon and (b) two tendons. All tendons with four strands 150 mm^2.

steps after appearance of the crack. The illustrated total crack opening t is almost constant over the height of the flanged girders SR21 and SR24 but slightly larger at mid-height. On the contrary, for specimen SR31 without flanges, crack opening varies over the height of the member, with a minimum value (no opening) near the compression chord and a maximum value near the tension chord (the main cracks in the web spread into several cracks with smaller openings in the tension chord, the opening of the latters are not drawn in Fig. 7c.

Just before peak load, the cracks of the flanged girders open almost vertically whereas for the girder without flanges a rotation around the crack tip develops. The total crack opening t is composed of a crack opening parallel to the crack surface w and a sliding Δ, leading for the direction of the total opening to an angle υ with respect to a direction normal to the crack surface (refer to Fig. 7d). Fig. 7e and f shows the crack opening of the critical crack at different load steps at the point P, which is selected at the girder axis. The crack opening at P exceeds a value of 0.5 mm at a load level V/V_R of about 0.80 and increases rapidly thereafter. The crack sliding also increases for all specimens with the level of applied load, particularly when the load level is larger than 70% of the failure one. This is represented by an increase on the value of the angle υ for increasing load levels.

3. Comparison to design codes

The measured shear strength of the test specimens is compared in this section to the prediction of various design codes in order to investigate on their accuracy. The selected design codes are Eurocode 2 [15], AASHTO LRFD [16], and Model Code 2010 [14].

As shown by various researches (refer for instance to [9,17]) and already implemented into many codes of practice, the presence of a post-tensioning duct has to be taken into account when assessing the compressive strength of the web of a girder. For the various codes investigated, the following reduced web thickness has been used:

$$t_{w,eff} = t_w - 0.5 \cdot \varnothing_{duct} \quad (1)$$

where coefficient 0.5 accounts for grouted steel ducts [17]. The web thickness is thus reduced by 25 mm which leads to an effective web thickness $t_{w,eff}$ of 125 mm for every beam with prestressing tendons. For the performed analyses, the formulas of the codes were used with the measured average values of the material properties of concrete, reinforcing steel and prestressing steel (see Tables 1 and 2) without any strength reduction factor. For the three codes, the requirements concerning the minimal shear reinforcement ratio are respected by the tested girders, except for beams SR23 and SR26 with the smallest amounts of 0.068% and for beam SR28 with a higher concrete strength. Nevertheless, they are considered in the comparison.

Fig. 8a–c shows the comparison of the test results to the codes. All design codes lead in general to conservative results with generally more accurate predictions for the flanged beams than for the girders without flanges. Details are given below.

Table 2
Measured reinforcing and prestressing steel properties.

Type	Ø (mm)	f_y (MPa)	f_t (MPa)	ε_u (%)
SR21, SR22, SR23, SR25, SR26, SR28, SR30				
Cold worked	6	585	640	3.1
Cold worked	8	549	615	4.3
Cold worked	10	565	620	1.8
Hot rolled	18	491	591	14.5
High strength	26	743	844	6.7
Strands	15.7	1689	1896	6.9
SR24, SR27, SR29				
Cold worked	6	575	623	2.9
Cold worked	8	540	603	3.9
Cold worked	10	571	618	3.8
Hot rolled	18	507	608	12.3
High strength	26	814	900	5.4
Strands	15.7	1724	1906	6.5
SR31, SR32				
Cold worked	6	525	588	5.6
Cold worked	8	555	607	4.3
Cold worked	10	538	600	5.6
High strength	26	743	844	6.7
Strands	15.7	1683	1910	6.6

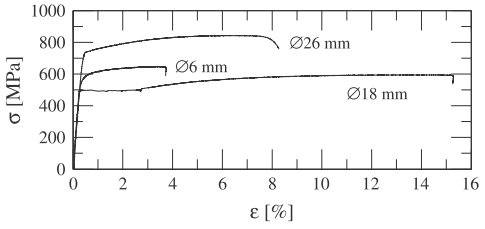

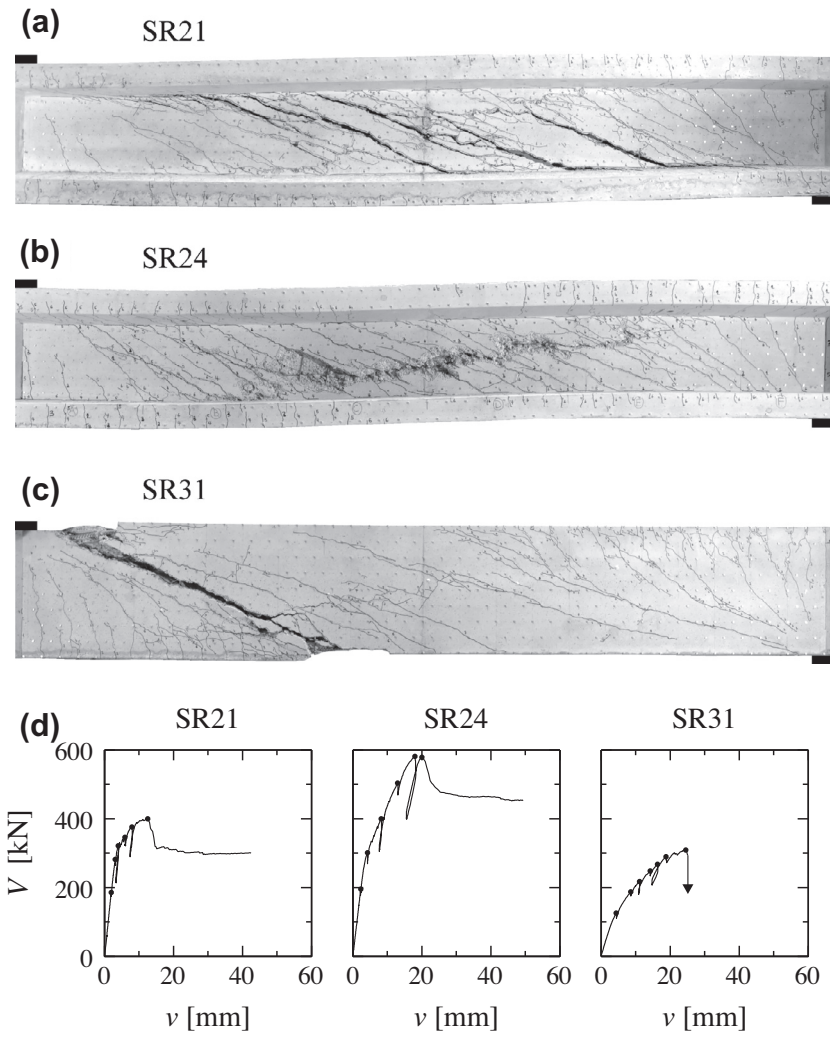

Fig. 4. Final crack pattern and concrete spalling in the testing region for three beams after failure: (a) SR21 – smeared cracking in the web with large openings and flange delamination; (b) SR24 – concrete crushing at the tendon region; (c) SR 31 – crack localisation; and (d) shear force (V) versus deflection (v) at the loading point in the span (x = 2600 mm) with indication of the load steps.

3.1. Eurocode 2

Eurocode 2 provisions use a classical variable angle truss model for shear design of members with shear reinforcement, where the stirrups contribute in tension and the concrete as inclined compression struts [18,19]. The shear strength measured for the different test specimens $V_{R,test}$ (Table 3) are divided by the corresponding shear strengths predicted by the code $V_{R,model}$ and presented in Fig. 8a. With an average value (Avg) of 1.44 and a coefficient of variation (CoV) of 16% over the panel of specimens, the results from

Table 3
Ultimate strength $V_{R,test}$, residual strength $V_{res,test}$, and predicted strength according to different models.

Beam	Failure mode (Fig. 4)	$V_{R,test}$ (kN)	$V_{res,test}$ (kN)	$V_{res,test}/V_{R,test}$ (–)	$V_{R,test}/V_{R,EC2}$ (–)	$V_{R,test}/V_{R,AASHTO}$ (–)	$V_{R,test}/V_{R,MC2010}$ (LoA III) (–)	$V_{R,test}/V_{R,EPSF}$ (–)
SR21	(a)	399	300	0.75	1.58	1.13	1.15	1.08
SR22	(b)	459	310	0.68	1.45	1.16	1.17	1.07
SR23	(a)	364	290	0.80	1.68	1.07	1.09	1.03
SR24	(b)	579	450	0.78	1.13	1.18	1.14	1.03
SR25	(b)	484	380	0.79	1.46	1.05	1.09	1.03
SR26	(a)/(b)	457	400	0.88	1.54	1.01	1.05	1.03
SR27	(b)	606	470	0.78	1.23	1.12	1.15	1.04
SR28	(a)	222	130	0.59	1.63	0.97	1.02	1.01
SR29	(b)	585	400	0.68	1.14	1.20	1.16	1.04
SR30	(b)	581	390	0.67	1.13	1.28	1.26	1.08
SR31	(c)	309	120	0.39	1.72	1.30	1.31	1.17
SR31B	(c)	303	90	0.30	1.69	1.28	1.29	1.14
SR32	(c)	173	90	0.35	1.36	0.86	0.91	0.99
Average					1.44	1.12	1.14	1.06
CoV					0.16	0.12	0.10	0.05

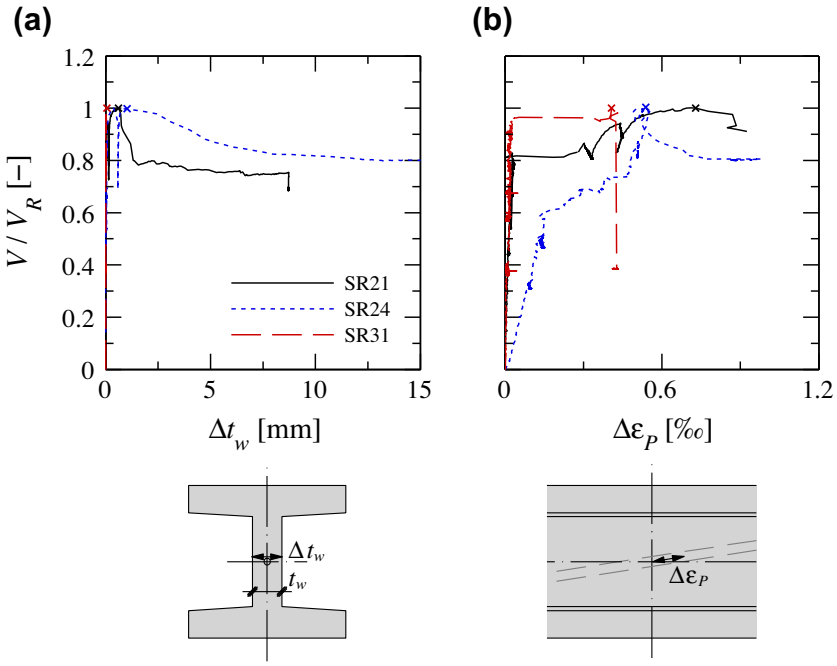

Fig. 5. Measured increase in (a) web thickness and (b) strain in prestressing tendon at the centre of the girder (x = 5000 mm) and at the height of the girder axis (z = 390 mm).

Eurocode 2 are rather conservative with the tendency to underestimate the shear strength of girders with lower amounts of shear reinforcement.

3.2. AASHTO LRFD

The shear design of the AASHTO LRFD Bridge Design Code is based on the Modified Compression Field Theory [13]. In this paper, the general shear design procedure has been used. The solution to the equations has been found by means of the spreadsheet available at [20]. The shear resistance consists of two parts, one carried by concrete and one carried by shear reinforcement, and has an upper limit to take into account the concrete crushing of the web. Fig. 8b shows the comparison of the code prediction with the test results. The average value $V_{R,test}/V_{R,model}$ over all specimens is 1.12 and the coefficient of variation is found to be 12%. The code leads in general to conservative results with a low overestimate of the shear resistance of 3% for the girder SR28 (no prestressing) and an overestimate of 14% for the girder SR32 (without flanges).

3.3. Model Code 2010

The Model Code 2010 provides three levels of approximation for the shear design and is based on the Generalized Stress Field Approach (GSFA [21]) and the Simplified Modified Compression Field Theory (SMCFT [22]) for members with transverse reinforcement (both sharing a common background). The first level of approximation (LoA I) represents a variable angle truss model as proposed in the Eurocode but with a safer estimate concerning the strut inclination θ_c. This LoA is aimed for preliminary design and checking of the dimensions of the web and will thus not be used in this paper for comparisons to tests. The second level (LoA II) is based on the GSFA with an inclination θ_c determined by longitudinal strains in the member. LoA II provides an average value $V_{R,test}/V_{R,model}$ of 1.41 and a coefficient of variation of 15% over all specimens. The approach is thus slightly more accurate than the one proposed in Eurocode but yet similar. The third level of approximation (LoA III) is based on both the GSFA and the SMCFT. The shear resistance consists of a shear reinforcement part and a concrete part (similar to AASHTO LRFD). The approach for the inclination of the compressive stress field is the same as used in LoA II. Fig. 8c shows the results of a comparison between the test results and the verification according to the LoA III of the Model Code. The average value $V_{R,test}/V_{R,model}$ over all specimens is found to be 1.14 with a coefficient of variation of 10%. The LoA III leads to conservative results for all tested beams, except for the girder SR32 (without flanges) where the shear strength is overestimated by 9%. The calculated inclination θ_c (based on longitudinal strain) varies from 20° for the beam SR26 with high post-tensioning force and the lowest amount of shear reinforcement to 28° for the beam SR30 with the highest amount of shear reinforcement and a reduced longitudinal reinforcement compared to the other specimens. This is thus the design model leading to better predictions of the strength.

4. Analysis of the specimens with elastic–plastic stress fields

The tested specimens have also been analysed with the elastic–plastic stress field (EPSF) method [11]. The EPSF method provides an equilibrium solution respecting the material failure criteria and respecting also the boundary and compatibility conditions. It leads thus to exact solutions according to the theory of plasticity (yet accounting for a strain-dependent concrete strength). All materials are modelled as having an elastic–plastic behaviour (without any strain limit in the plastic domain) using the measured material properties for concrete, reinforcing steel and prestressing steel (see Tables 1 and 2).

The concrete compressive strength is reduced by a strength reduction factor η_ε which accounts for the tensile strains (and cracking state) in the transverse direction to the compression field [13] and by a factor η_{fc} accounting for concrete brittleness [12]. The latter coefficient allows the use of plastic analyses (with redistribution of stresses within concrete) and can be estimated as [12]:

$$\eta_{fc} = (30/f_c)^{1/3} \leqslant 1.0 \qquad (2)$$

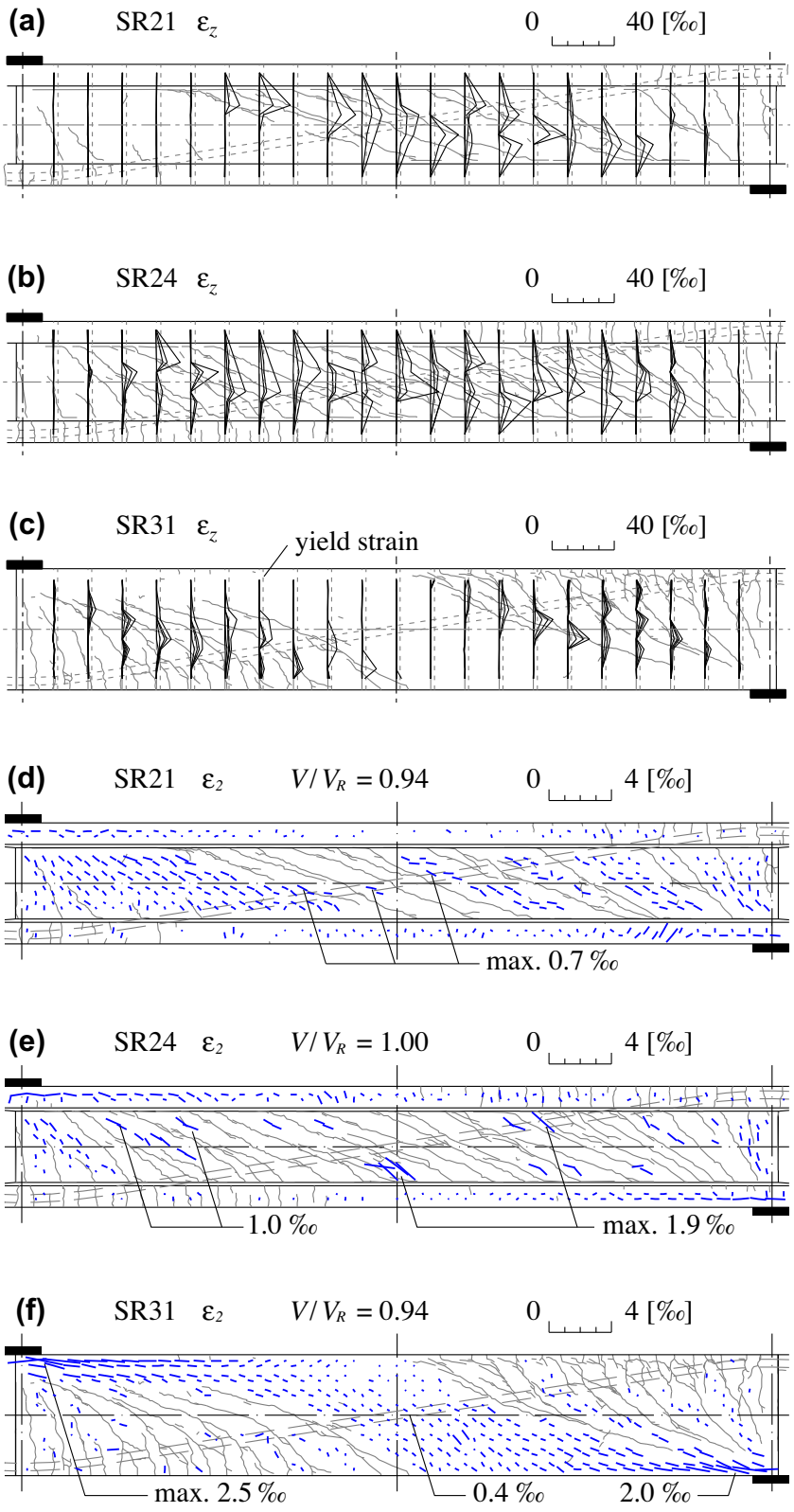

Fig. 6. Measured vertical strains ε_z in the testing region at different load steps (only cracks present before peak load are drawn): (a) SR21 at load levels of 71%, 80%, 86% and 94% of the peak load; (b) SR24 at load levels of 52%, 69%, 87% and 100% of the peak load; (c) SR31 at load levels of 61%, 70%, 80%, 86% and 94% of the peak load. Measured concrete compressive strains ε_2 in the testing region at the last load step: (d) SR21; (e) SR24; (f) SR31.

The model assumes a fully-rotational cracking behaviour and that the principal directions of the stress and strain tensors are parallel ($\theta_\sigma = \theta_\varepsilon = \theta_{crack}$) [11]. The actual geometry and boundary conditions are considered by modelling the structure through a finite element

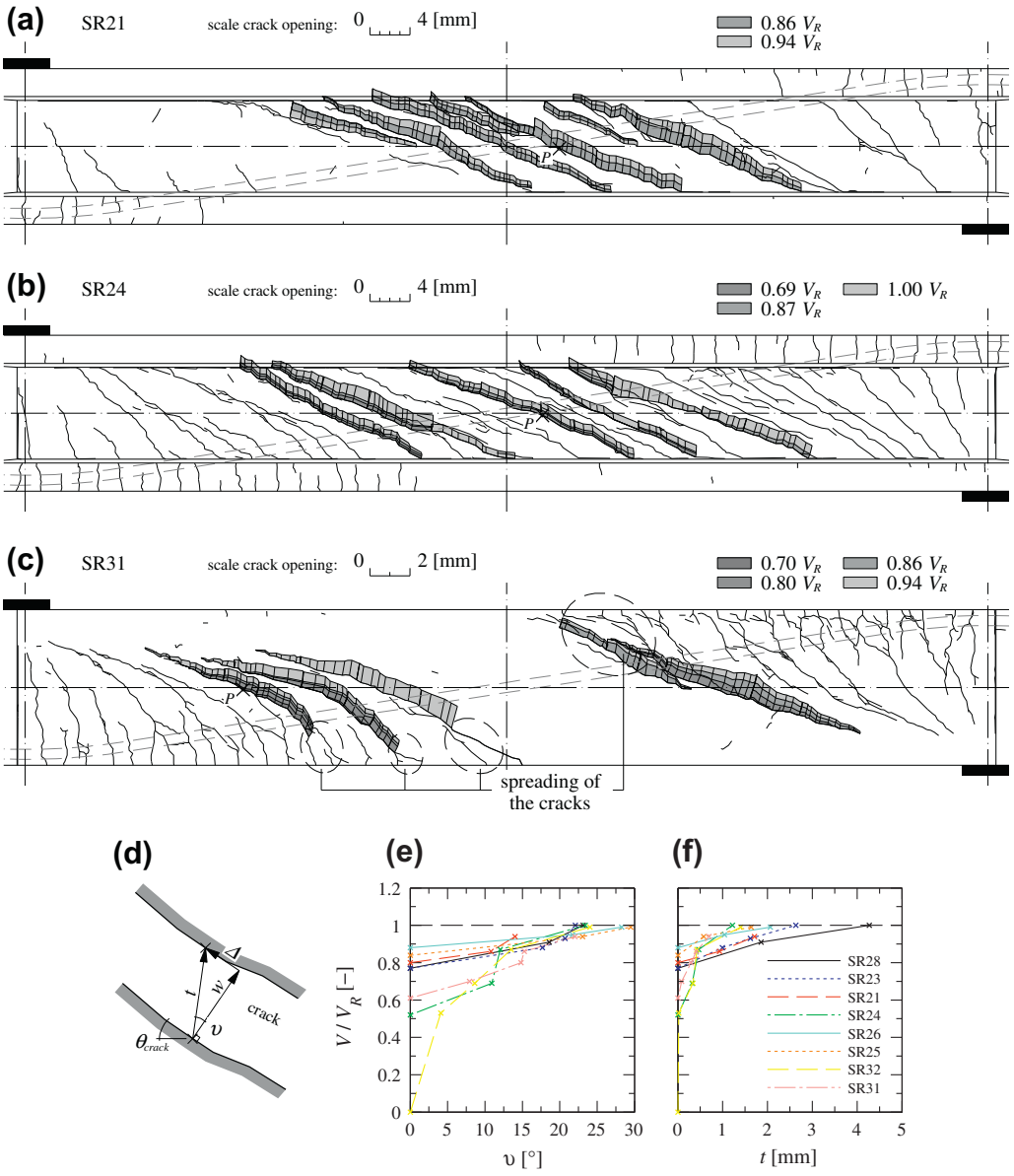

Fig. 7. Kinematics of the measured crack opening for several cracks (only cracks present before peak load are drawn): (a) SR21; (b) SR24; (c) SR31; (d) components of the total crack opening t normal to the crack surface w and sliding parallel to the crack surface Δ. Direction of the crack opening υ (e) and crack opening t (f) at different load stages on the location P of various specimens.

mesh. To account for the presence of tendons, the web thickness is reduced in this region by half of the tendon diameter (Eq. (1)) to an effective value $t_{w,eff}$ of 125 mm. More details on this technique can be found elsewhere [9].

4.1. Analysis of EPSF results

The results of the EPSF analysis are presented in Table 3 and Fig. 8d. With an average value $V_{R,test}/V_{R,model}$ of 1.06 and a coefficient of variation of 5% the accuracy of the method is very satisfying and has a similar accuracy to that of similar analyses on other prestressed girders [9]. The model provides conservative estimates for all specimens, apart from the girder SR32 where the strength is overestimated by 1%. In general, the prediction is very accurate for the beams with flanges where the average value $V_{R,test}/V_{R,model}$ is found to be 1.04 and the coefficient of variation 2% only.

4.2. Interpretation of test results on the basis of EPSF

Fig. 9c–e shows the measured and calculated angles θ_ε of the principal compressive strains. They are plotted in the testing region, at mid-height of the specimen, and for the three beams SR21, SR24 and SR31 (the measurements show a certain scatter due to the cracks developing between measurement points). The value of θ_ε corresponds in the uncracked regions (dots in Fig. 9c–e) to the inclination of the principal concrete stress θ_σ whereas in the cracked zone θ_ε deviates due to crack sliding. It can be noted that EPSF analyses are based on a fully-rotational cracking behaviour without crack sliding and thus they assume that the principal direction of strain and stress are always coincident ($\theta_\varepsilon = \theta_\sigma$). The comparison of measured and calculated angles shows a rather good agreement, validating the use of the EPSF method for modelling the strain state of the specimens of the present test series. The variation of the angle near the loads is justified by the fans distributing the load to the required number of stirrups (refer to the elas-

tic–plastic stress field shown in Fig. 9a, and to the rigid-plastic stress field and the strut-and-tie model in Fig. 9b [12]). Between the two fans, a region with a parallel stress field develops (the angle of the compression field is found fairly constant). The minimum value of the angle varies between 13.6° (low ρ_w) to 19.8° (high ρ_w), in fine agreement to the test results and clearly showing the influence of the amount of transverse reinforcement on the angle of the compression field of the web (Fig. 9f). Prestressing seems to play a more secondary role on the inclination of the compression field (Fig. 9g), although it influences other parameters (as the strength reduction factor accounting for the cracking state of concrete η_ε).

Fig. 10 presents the analysis results for the three beams SR21, SR24 and SR31 representing the three different failure modes, which can be identified by analysing the results. Some interesting observations are:

- For the girder SR24 the Fig. 10b shows clearly the spalling of the concrete along the tendon axis (out-of-plane failure in a region near mid-span, cf. Fig. 4). The principal concrete compressive stress reaches in various elements the concrete strength (ratio

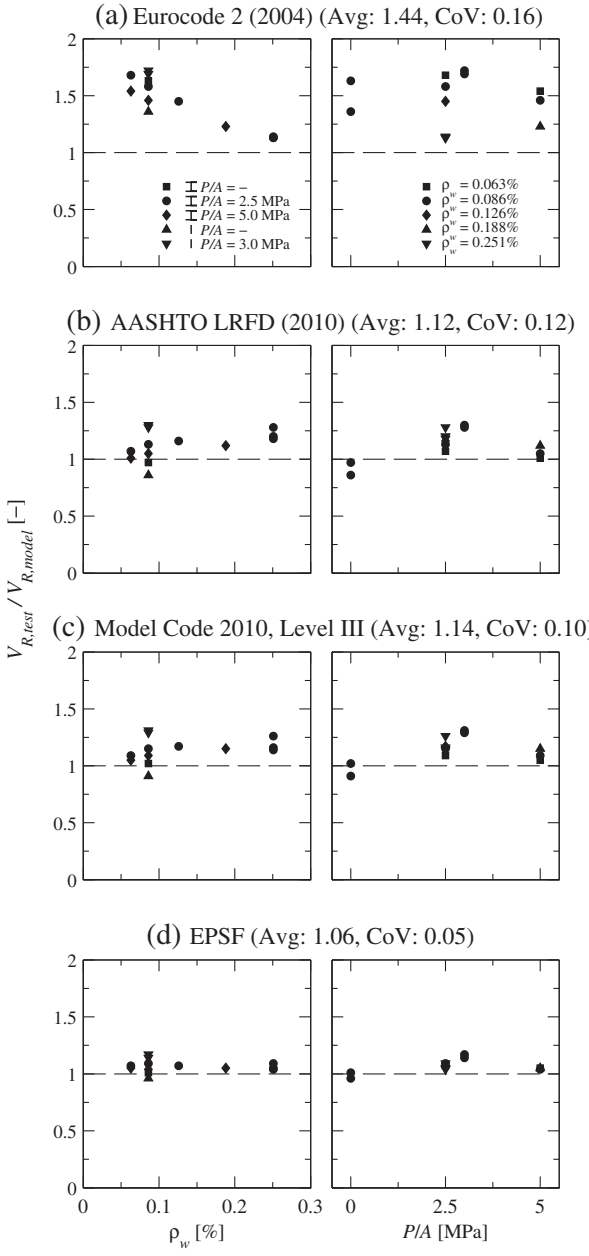

Fig. 8. Ratio of $V_{R,test}/V_{R,model}$ for different models versus the amount of shear reinforcement and the prestressing ratio: (a) Eurocode 2 (2004); (b) AASHTO LRFD (2010); (c) Model Code 2010, Level III; (d) elastic–plastic stress fields.

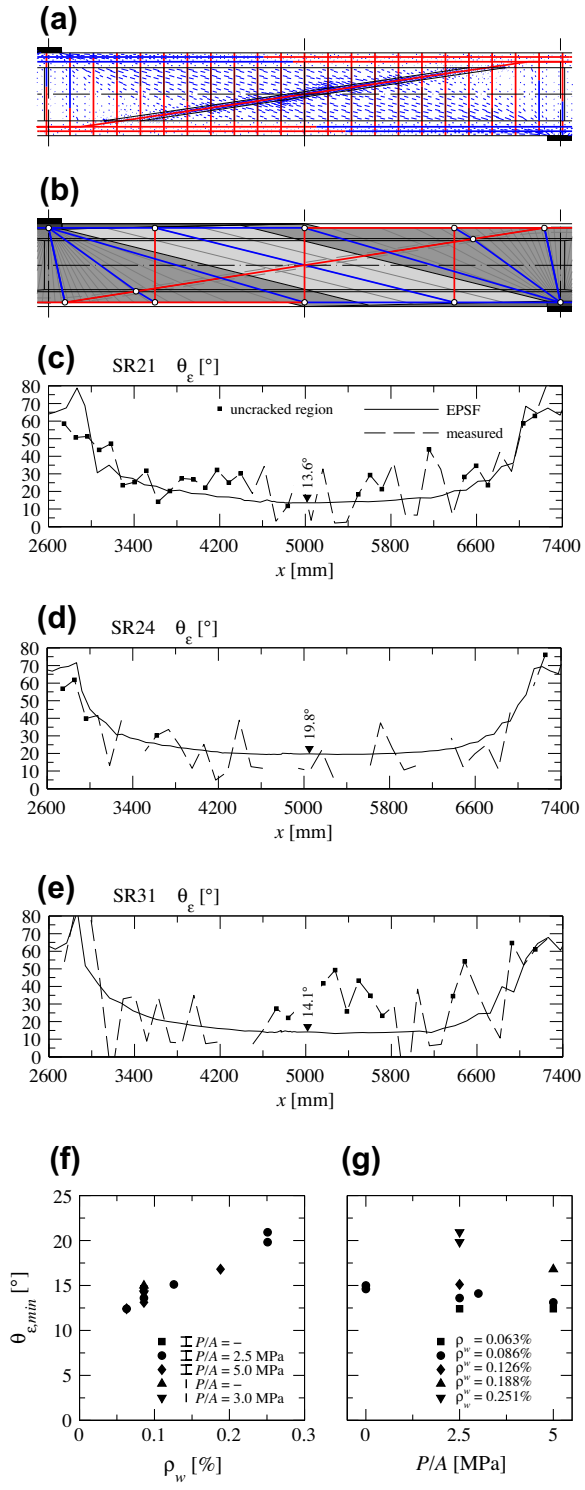

Fig. 9. (a) Elastic–plastic stress field, (b) rigid-plastic stress field with corresponding strut-and-tie model for girder SR21. Comparison of measured and calculated principal strain angle θ_ε (c–e) at $z = 360$ mm (30 mm lower than the longitudinal girder axis, only the testing region is presented). Minimal calculated inclination θ_ε at the middle of the beam and at mid-height ($x = 5000$ mm, $z = 360$ mm) versus amount of shear reinforcement (f) and versus nominal prestressing ratio (g) for all girders.

$\sigma_c/(\eta_\varepsilon \cdot \eta_{fc} \cdot f_c) = 1$) whereas the maximal tensile strains in the transverse reinforcement ε_z are slightly above their yield threshold (Fig. 10f). The inclination of the principal compressive strains θ_ε in the web varies along the x-direction and reach a minimum value of 19.8° in the middle of the beam (x = 5000 mm, Fig. 10c) similar to the inclination assumed in the design codes. The minimum strength reduction factor accounting for transverse cracking η_ε (calculated according to Vecchio and Collins [13]) is found to be 0.6 (Fig. 10 (d)) in close agreement to the usual reduction proposed by codes of practice.

– The principal concrete compressive stresses in girder SR21 are smaller than the concrete strength $\eta_\varepsilon \cdot \eta_{fc} \cdot f_c$, except at the interface between the flange and the web near the load introduction points (Fig. 10b). This is exactly the region where in the test the delamination cracks could be observed (in-plane failure with delamination, cf. Fig. 4). In contrast to the girder SR24, the maximal tensile strains in the transverse reinforcement ε_z reach higher values of 0.8% indicating stirrups close to tensile rupture (Fig. 10f, Table 2). The region (bandwidth) of these higher strains corresponds to the zone with large crack opening observed in the test (cf. Fig. 4). The inclination of the principal compressive strains θ_ε in the web reach a minimum value of 13.6° in the middle of the beam (x = 5000 mm, Fig. 10c) significantly lower than that assumed by design codes but in good agreement to the test results. The minimum strength reduction factor due to transverse cracking η_ε is found to be 0.5 (Fig. 10d) slightly lower than usual design values (η_ε = 0.6).

– For the girder SR31 Fig. 10b and f indicate failure by crushing of the compression zone in a localised region (band) with extensive stirrup elongation at the same location, which corresponds to the observed behaviour of the specimen. The inclination of the principal compressive strains θ_ε in the web reach a minimum value of 14.1° (Fig. 10c) very low compared to those of codes but in agreement to the demec measurements (Fig. 9c). The minimum strength reduction factor due to transverse cracking η_ε is found to be 0.4 (Fig. 10d) significantly lower than the one assumed for typical design [9].

The elastic–plastic stress field model allows in addition investigating the various shear carrying actions of the beams, which are presented in Fig. 11. The various actions considered are: the shear force carried by the flanges, the shear force carried by the web (region between flanges) and the shear force carried by the tendons (including its initial component as well as its increase as the members deforms). Fig. 11a and b shows the various contributions to the shear strength of the girder SR21 as a percentage of the total shear force. The contributions to the shear strength in the middle of the testing region are plotted for all tested girders in Fig. 11c.

With respect to the flanges, they transfer between 10% and 15% of the total shear force over a large region of the beam and for vary-

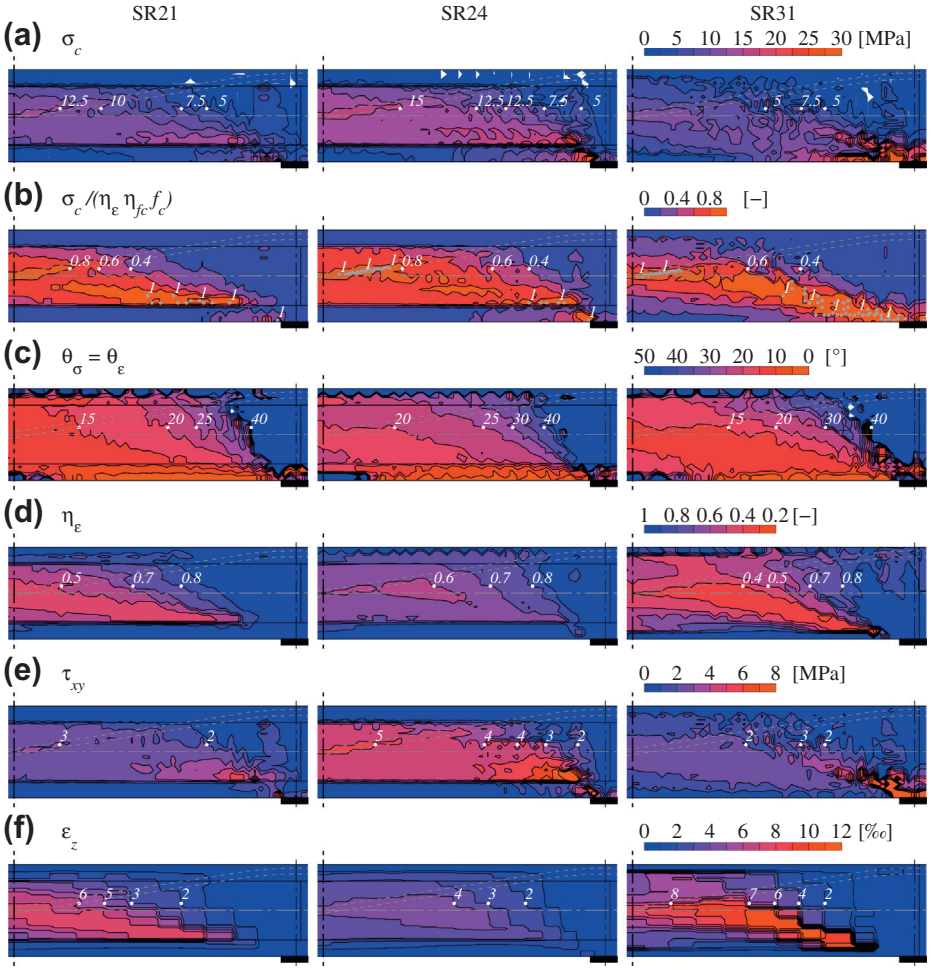

Fig. 10. Analysis results of the elastic–plastic stress fields method for the girders SR21, SR24 and SR31 at peak load (only half of the testing region is presented): (a) principal concrete compressive stress σ_c; (b) concrete compressive stress σ_c divided by the equivalent plastic strength $\eta_\varepsilon\ \eta_{fc}\ f_c$; (c) inclination of the compression field θ_σ (=θ_ε; (d) strength reduction factor η_ε for the concrete (calculated according to [13]); (e) shear stress τ_{xy} in the direction of the girder axes; (f) tensile strain in the stirrups ε_z.

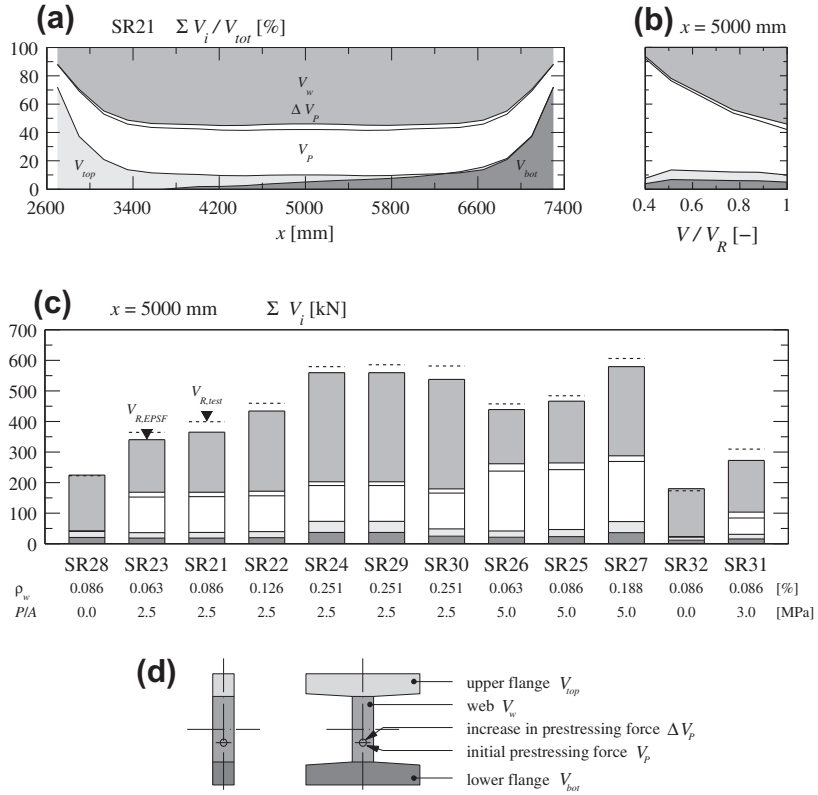

Fig. 11. Shear force carried by different elements of the cross-section: (a) variation of shear force at peak load over length of the girder SR21 (only the testing region is presented) and (b) variation over different load stages at the middle of the girder SR21 (x = 5000 mm); (c) shear force at peak load carried by the different specimens at the middle of the girder (x = 5000 mm); (d) definition of the different shear carrying elements.

ing load levels (which is consistent with the results on the same topic presented elsewhere [9]). It has to be noted that a part of this shear force carried by the flanges is taken also into account in codes of practice due to the different definition of the height of the web (codes usually consider the height of the web between axes of the tension and compression chord and not between flanges).

The shear force carried by the flanges is of increasing significance close to the loading regions due to the fact that the shear carrying compression strut under the load develops through the flange (refer to the strut-and tie model of Fig. 9b). In addition, the influence of the flanges can still be observed at a certain distance (for instance about 800 mm from the loading plate in girder SR21 according to Fig 11a), due to the capacity of the flange to carry shear forces (due to its stiffness), spreading the load over a larger distance. This effect leads in these regions close to the loading points to a smaller shear force carried by the web and for the verification according to design codes, to a potentially different control section (farther from the loading points). This, in combination to the cracking state (refer to coefficient η_ε of Fig. 10d) has significant practical consequences, as for some design models (as AASHTO LRFD and Model Code 2010) the shear strength depends on the bending moments (associated to the longitudinal strains of the member). A change in the location of the control section leads thus to different bending moments and to a different shear strength. In the case of the investigated specimens, the two design codes use a control section at a distance between $0.5 \cdot z \cdot \cot\theta$ (AASHTO LRFD) and d (Model Code 2010). It can be noted that other potential control sections could be governing according to the codes depending on the inner forces and geometric discontinuities. However, for the investigated specimens, the governing control sections are located at the closest possible location (accounting for the distances previously mentioned) to the introduction of the loads, where shear force is constant and the bending moments (associated to larger longitudinal strains and crack widths) are larger. These control sections given by the codes do not correspond to the actual failure regions, which are located in the middle of the testing region (except for members without flanges), where the bending moments are almost equal to zero. Contrary to these models, the analyses on the basis of EPSF suitably capture the role of the flanges and the location of the failure region.

In addition, comparing specimens SR21 and SR31 with similar characteristics (refer to Table 1), one presenting flanges and the other not, it can be noted that the presence of flanges modify the failure mode (from a localised cracking and a brittle behaviour (SR31) to a smeared cracking with extensive yielding of the stirrups (SR21)). This can be explained by the fact that the flanges allow redistributing the load (as they carry a fraction of shear) avoiding strain localisation. This effect is thus very beneficial for the overall behaviour of the member and can also be observed for the post-peak response.

The maximum compressive strains measured and calculated through EPSF for the various specimens show different behaviours depending on the failure modes. When the member experiences an out-of-plane failure with crushing of concrete localised in the tendon region, the compressive strains can be quite high (close to 2‰). This value is nicely similar to that assumed by some codes of practice as Model Code 2010 when crushing of the compression field is governing. However, for members where failure develops by in-plane failure of concrete (associated to very large crack opening), the actual strains (measured and calculated through EPSF) in the concrete are quite low (0.7‰ for members with flanges, 0.4‰ for members without flanges, excluding the flexural chord region for the latter), significantly smaller than those assumed by design

codes at web crushing. This implies that the design formulas of codes may not, at least from a phenomenological point of view, be suitable for reproducing all failure modes.

With respect to the prestressing force, Fig. 11c shows for all prestressed girders a certain increase in the prestressing force at failure, which is usually neglected for design of such members according to design codes. The shear force carried by this increase in prestressing force ΔV_P varies between 2.3% and 7.2% of the total shear strength. The measurements of the prestressing strain (refer to Fig. 5b) confirm this increase in force and lead for most of the girders to similar values. The increase in prestressing force is yet moderate for the tested girders. Nevertheless, the increase in prestressing force can be potentially significant for other regions (near plastic hinges).

5. Conclusions

This paper presents the results of an experimental programme on post-tensioned concrete beams with low amounts of shear reinforcement, investigating also the role of the flanges on their behaviour and strength. The test results are compared to the predictions of different codes of practice and to the results of elastic–plastic stress fields. The main findings of the experimental investigation are:

1. The shear strength and the failure mode of prestressed concrete girders are significantly influenced by the amount of shear reinforcement, the level of post-tensioning force, and the presence of flanges.
2. Three different failure modes could be observed in the test series. Flanged beams with higher amounts of shear reinforcement failed by an out-of-plane failure of concrete along the tendons. Flanged girders with lower amounts of shear reinforcement failed by an in-plane failure with extensive cracking of the web, flange delamination, and rupture of the stirrups in the cracks. The third failure mode could be observed for beams without flanges and low amounts of transverse reinforcement, where a localisation of the deformations in a single crack occurred.
3. All flanged beams showed a significant residual strength after peak load, independently of the failure mode. On the contrary, girders without flanges failed in a brittle manner with low residual strength. Therefore, the flanges of the girders turn out to be very beneficial for structural safety as they increase the residual strength of the members.
4. The measured kinematics in the web indicates that for high load levels, cracks in the web open almost vertically, associated to significant crack sliding.

The comparison of the test results to codes of practice and to elastic–plastic stress fields (EPSF) lead in addition to the following conclusions:

5. The investigated design codes provide in general conservative but yet fairly accurate estimates for the strength of the girders tested in the experimental programme. The EPSF analyses leads to the most accurate predictions and provides additional information on the failure mode, the contribution of the various shear transfer actions, or the actual strain state in the girders. The values obtained by the EPSF method are in fine agreement to the performed measurements.
6. The comparison of design codes to test results as well as the EPSF analysis and the observed failures confirm the pertinence of reducing the web thickness for shear design in presence of post-tensioning ducts.
7. The measurements on the tested girders as well as the stress field analysis show discrepancies between some assumptions adopted in codes of practice and the actual behaviour of the girders:
- The flanged girders failed in the middle of the testing region whereas codes requiring a control section for shear design place it near the loading points (generally at a distance between half and one time the lever arm of internal forces). This location, which is not suitably estimated by the codes, is significant as it is associated to a bending moment which in turn influences the shear strength estimated by the codes.
- Flanges carry a significant fraction of the load near loading points. This, together with the actual angle of the compression struts, explain the shift of the control section to regions farther from the loading points.
- The presence of flanges modifies the failure mode from a localised cracking and a brittle behaviour to a smeared cracking with extensive yielding of the stirrups. This can be explained by the fact that the flanges allow redistributing the load (as they carry a fraction of shear) avoiding strain localisation. This effect is thus very beneficial for the overall behaviour of the member and can also be observed for the post-peak response.
- The states of strains of the tested girders differ for the various observed failure modes. For out-of-plane failures (crushing localised at the tendon region), the maximum compressive strength is similar to 2‰, the same value assumed by several codes of practice at concrete crushing. For in-plane failures of concrete, these strains are however significantly lower (0.4–0.7‰) and in disagreement to the values assumed by these codes.
- An increase of stresses in the prestressing tendons has been consistently measured. Such increase can be lead to transfer between 2.3% and 7.2% of the total shear force at failure for the tested girders. This fact is commonly neglected for design in most codes of practice, and may be significant particularly for failures near plastic hinges (or regions where tendons are highly elongated at failure).

Acknowledgments

The authors like to thank the Swiss Federal Roads Office FEDRO for the funding of the presented research and the experimental programme.

References

[1] Caflisch R, Thürlimann B. Shear Tests on partially prestressed concrete girders. In: German: Schubversuche an teilweise vorgespannten Betonbalken, Institut für Baustatik und Konstruktion. ETHZ, Zürich, Switzerland; 1970. 177p.
[2] Bennett EW, Balasooriya BMA. Shear strength of prestressed beams with thin webs failing in inclined compression. ACI J. 1971;68:204–12.
[3] Leonhardt F, Koch R, Rostásy FS. Shear tests on prestressed concrete girders. In: German: Schubversuche an Spannbetonträgern, Deutscher Ausschuss für Stahlbeton, vol. 227. Berlin, Germany: Heft; 1973. 179p.
[4] Moayer H, Regan PE. Shear strength of prestressed and reinforced concrete T-beams. ACI Spec Publ 1974;42:183–221.
[5] Feddersen B, Nielsen MP. Bent-up prestressing as shear reinforcement. In: Danish: Opbøjet spændarmering som forskydningsarmering. Technical University of Denmark, Serie R, No. 160. Lyngby, Denmark; 1983. p. 33.
[6] Gregor T, Collins MP. Tests of large partially prestressed concrete girders. ACI Struct J 1995;92(1):63–72.
[7] Kaufmann W, Marti P. Tests on reinforced concrete girders under normal and shear force. In: German: Versuche an Stahlbetonträgern unter Normal- und Querkraft, Institut für Baustatik und Konstruktion, ETHZ. Zürich, Switzerland; 1996. 141p.
[8] Hegger J, Sherif A, Görtz S. Investigation of pre- and postcracking shear behavior of prestressed concrete beams using innovative measuring techniques. ACI Struct J 2004;101(2):183–92.
[9] Fernández Ruiz M, Muttoni A. Shear strength of thin-webbed post-tensioned beams. ACI Struct J 2008;105(3):308–17.

[10] Kuchma D, Kim KS, Nagle TJ, Sun S, Hawkins NM. Shear tests on high-strength prestressed bulb-tee girders: strengths and key observations. ACI Struct J 2008;105(3):358–67.
[11] Fernández Ruiz M, Muttoni A. On development of suitable stress fields for structural concrete. ACI Struct J 2007;104(4):495–502.
[12] Muttoni A, Schwartz J, Thürlimann B. Design of concrete structures with stress fields, Birkhäuser. Boston and Berlin, Switzerland: Basel; 1997. 145p.
[13] Vecchio FJ, Collins MP. The modified compression field theory for reinforced concrete elements subjected to shear. ACI J Proc 1986;83(2):219–31.
[14] fib Fédération international du béton, Model Code 2010, Final Draft, Lausanne, Switzerland; 2010. 653p.
[15] CEN European Committee for Standardization, Eurocode 2. Design of concrete structures – general rules and rules for buildings, EN 1992-1-1, Brussels, Belgium; 2004. 225p.
[16] AASHTO LRFD, Bridge design specifications and commentary. 5th ed. Washington, DC, USA: American Association of State Highway Transportation Officials; 2010.
[17] Muttoni A, Burdet O, Hars E. Effect of duct type on the shear strength of thin webs. ACI Struct J 2006:729–35.
[18] Nielsen MP, Braestrup MW, Bach F. Rational analysis of shear in reinforced concrete beams. In: IABSE colloquium proceedings, P-15, vol. 2. Bergamo, Italy; 1978. 16p.
[19] Thürlimann B. Shear strength of reinforced and prestressed concrete-CEB approach. ACI Spec Publ 1979;59:93–116.
[20] Bentz E, Collins MP. Spreadsheet to calculate the shear strength according to AASHTO code. Canada: University of Toronto. <http://www.ecf.utoronto.ca/~bentz/aashto99.htm>.
[21] Sigrist V. Generalized stress field approach for analysis of beams in shear. ACI Struct J 2011;108(4):479–87.
[22] Bentz EC, Vecchio FJ, Collins MP. Simplified modified compression field theory for calculating shear strength of reinforced concrete elements. ACI Struct J 2006;103(4):614–24.